

# Nanoscale

Accepted Manuscript



This is an *Accepted Manuscript*, which has been through the Royal Society of Chemistry peer review process and has been accepted for publication.

*Accepted Manuscripts* are published online shortly after acceptance, before technical editing, formatting and proof reading. Using this free service, authors can make their results available to the community, in citable form, before we publish the edited article. We will replace this *Accepted Manuscript* with the edited and formatted *Advance Article* as soon as it is available.

You can find more information about *Accepted Manuscripts* in the [Information for Authors](#).

Please note that technical editing may introduce minor changes to the text and/or graphics, which may alter content. The journal's standard [Terms & Conditions](#) and the [Ethical guidelines](#) still apply. In no event shall the Royal Society of Chemistry be held responsible for any errors or omissions in this *Accepted Manuscript* or any consequences arising from the use of any information it contains.

## Figures and Captions

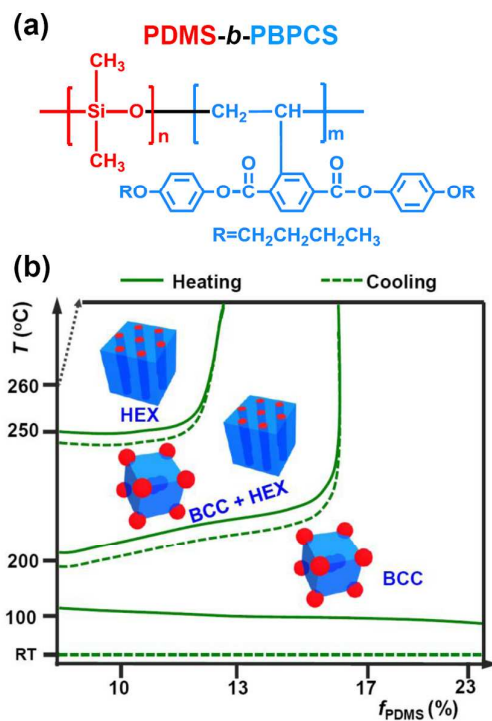


**Fig. 1** (a) Chemical structure of the PDMS-*b*-PBPCS block copolymers and (b) the nanophase-separated structures in bulk with varying compositions in different temperature ranges.

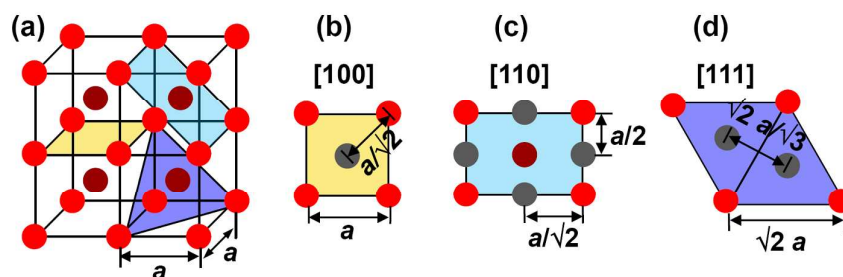


**Fig. 2** (a) The model of the BCC structure and (b–d) the models of the patterns which can be observed perpendicular to the corresponding planes of the BCC structure including [100], [110], and [111] zones.

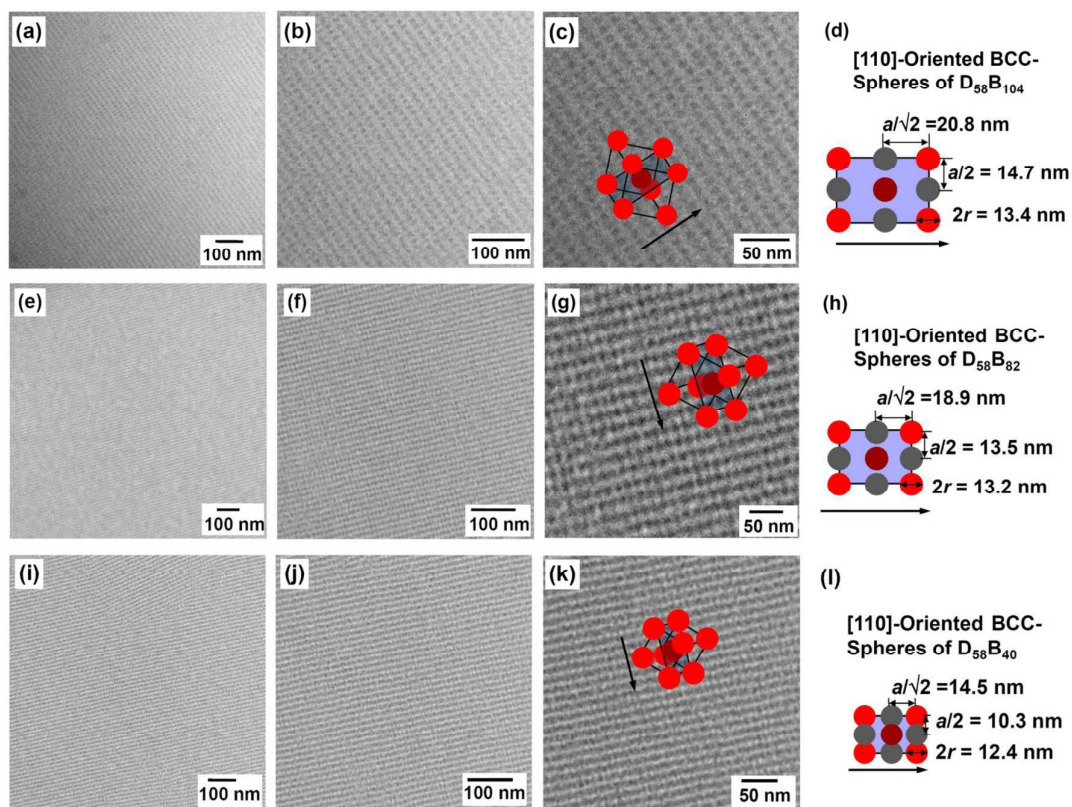


**Fig. 3** (a–c) TEM micrographs with different magnifications of [110]-oriented BCC-spheres in the thin film of  $D_{58}B_{104}$  (inset of c is the model of the orientation of the BCC structure), and (d) the model of the pattern observed by TEM along the [110] direction of the BCC structure. And the corresponding TEM micrographs and models of (e–h)  $D_{58}B_{82}$  and (i–l)  $D_{58}B_{40}$ .

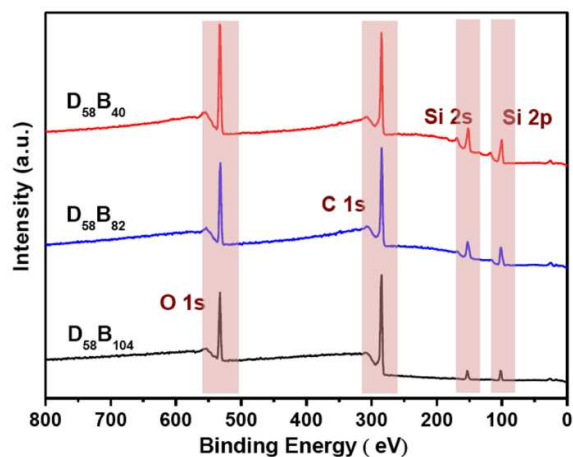


**Fig. 4** XPS spectra of the thin films of  $D_{58}B_{104}$ ,  $D_{58}B_{82}$  and  $D_{58}B_{40}$  BCPs.

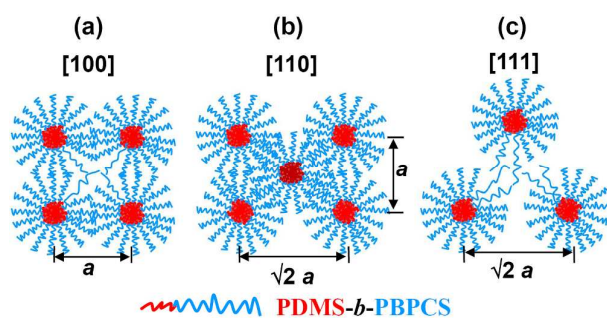


**Fig. 5** The schematic representation of chain arrangements of the DB block copolymer in a single [100] (a), [110] (b), and [111] plane (c) of the BCC structure, respectively.

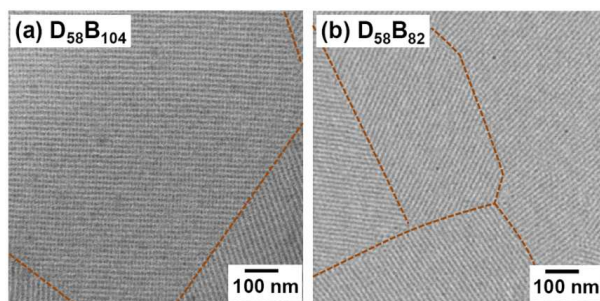


**Fig. 6** TEM micrographs of thin films with several [110]-oriented BCC domains of (a)  $D_{58}B_{104}$  and (b)  $D_{58}B_{82}$ . The boundaries of adjacent domains are indicated with dashed lines.

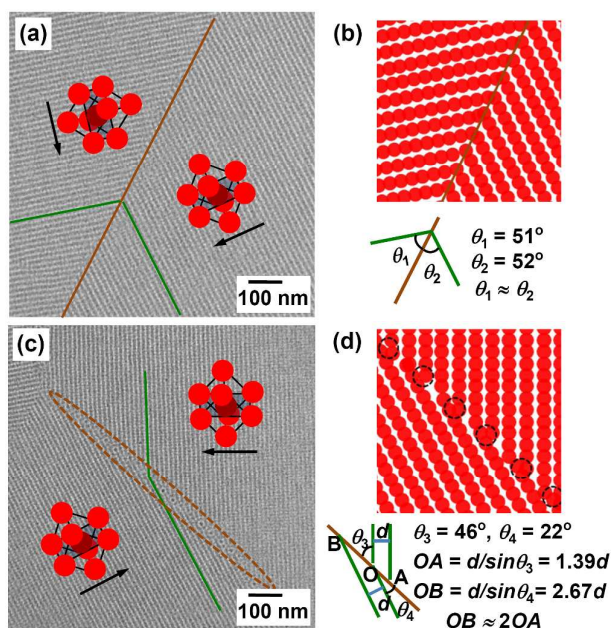


**Fig. 7** (a) TEM micrograph of symmetrically oriented [110] domains in the thin film of  $D_{58}B_{40}$  and (b) the corresponding model of the arrangement of PDMS dots. (c) TEM micrograph of the thin film of  $D_{58}B_{40}$  with asymmetrically oriented [110] domains and (d) the corresponding model of the arrangement of PDMS dots.

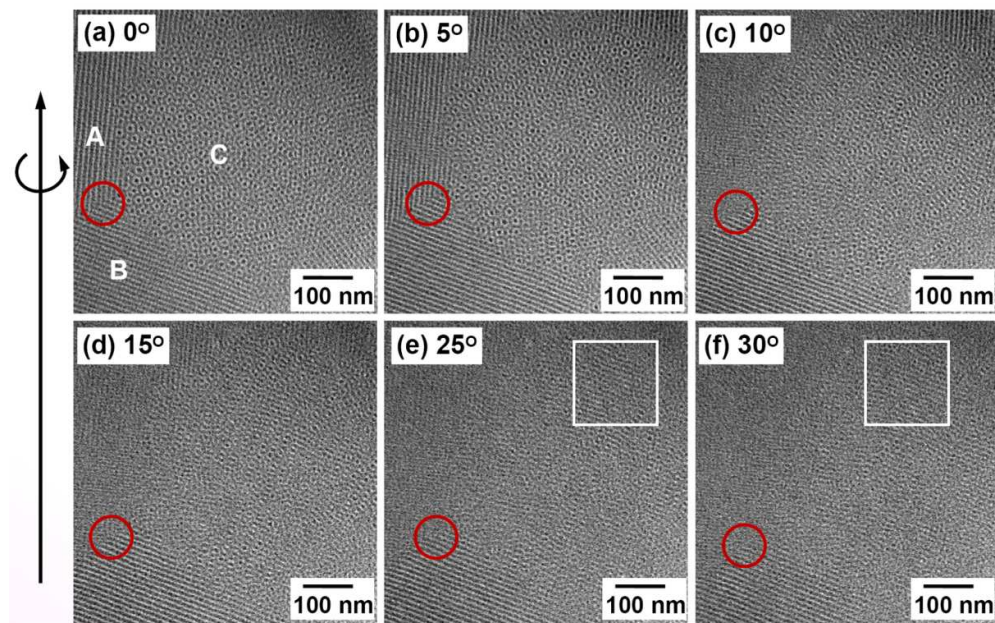


**Fig. 8** TEM micrographs of  $D_{58}B_{40}$  for the structural determination at tilting angles of (a–f)  $0^\circ$ ,  $5^\circ$ ,  $10^\circ$ ,  $15^\circ$ ,  $25^\circ$ , and  $30^\circ$ . The joint of three domains used as a reference marker is circled in each micrograph.

**Table 1.** Molecular Weights, Polydispersity Indexes,  $f_{\text{PDMS}}$  Values of the DB Samples, and  $T_g$  Values of PBPCS Blocks, as Well as Nano-structure Characteristics of the Diblock Copolymers after Thermal Annealing in Vacuum at 180 °C for 48 h

Sample	$M_n^a$ (g/mol)	PDI <sup>a</sup>	$f_{\text{PDMS}}^b$ (%)	$T_{\text{g(PBPCS)}}^c$ (°C)	$q^{*d}$ (nm <sup>-1</sup> )	$d$ (nm)	Nanostructure
D <sub>58</sub> B <sub>104</sub>	30,200	1.09	10	110	0.302	20.8	BCC
D <sub>58</sub> B <sub>82</sub>	24,300	1.09	13	108	0.333	18.9	BCC
D <sub>58</sub> B <sub>40</sub>	11,300	1.08	23	102	0.433	14.5	BCC

<sup>a</sup> Determined from gel permeation chromatography results using linear polystyrene standards. <sup>b</sup> Determined from <sup>1</sup>H NMR results of the block copolymers. Correspondingly, the values of polymerization degree of the PBPCS block labeled in the subscripts of the sample names were calculated from the molecular weights determined from <sup>1</sup>H NMR results. <sup>c</sup> Determined from differential scanning calorimetry experiment results. <sup>d</sup> Determined from small angle X-ray scattering experiment results.



Journal Name

ARTICLE

## Extraordinary Boundary Morphologies of Large-Scale Ordered Domains of Spheres in Thin Films of a Narrowly Dispersed Diblock Copolymer via Thermodynamic Control

Received 00th January 20xx,  
Accepted 00th January 20xx

DOI: 10.1039/x0xx00000x

www.rsc.org/

Ling-Ying Shi,<sup>\*a</sup> Hang Li,<sup>a</sup> Wei-Wei Lei,<sup>a</sup> Wei Ni,<sup>a</sup> Rong Ran,<sup>a</sup> Yu Pan,<sup>b</sup> Xing-He Fan<sup>b</sup> and Zhihao Shen<sup>b</sup>

Long-range ordering of body centered cubic (BCC) spheres and various extraordinary morphologies at boundaries of adjacent orderly oriented domains are observed in thermally annealed thin films of a series of specific narrowly dispersed diblock copolymers, poly(dimethylsiloxane)-*b*-poly{2,5-bis[(4-butoxyphenyl)oxycarbonylstyrene]} (PDMS-*b*-PBPCS, DB). The series of asymmetrical DB block copolymers (BCPs) with volume fractions of PDMS ( $f_{\text{PDMS}}$ 's) from 10% to 23% self-assemble into thermodynamically stable body centered cubic (BCC) nanostructures in bulk at ambient temperature after thermal annealing. The thin films of these BCPs with relatively large film thickness on carbon-film coated substrate are annealed in vacuum at 180 °C for 3 days and are characterized by transmission electron microscopy (TEM) and X-ray photoelectron spectroscopy (XPS). For all thin films of these BCPs, micrometer-scale domains with a rectangular unit cell similar to the projection of the BCC lattice along the [110] direction to the substrate are observed. And the XPS results indicate that the surface layers of the thin films are composed of both PDMS and PBPCS blocks. For the thin films of the BCPs with  $f_{\text{PDMS}}$  values of 10% and 13%, the neighboring [110]-oriented BCC domains match well with each other, and the boundaries are defect-free. For the thin film of the BCP with a  $f_{\text{PDMS}}$  value of 23%, the PDMS spheres in the [110]-oriented BCC domains in the TEM micrograph are overlapped with each other, and interesting morphologies including defect-free interfaces, interfaces with line defects, and domains with defects and local ordering are observed at the boundaries of the neighboring [110]-oriented domains.

### Introduction

Block copolymers (BCPs) have great potential applications in nano-technology owing to their capability of providing various periodic nanostructures.<sup>1-3</sup> In particular, BCP thin films with long-range ordered nanostructures can be applied in many fields such as nanolithography, separation membranes, and nano-scale templates.<sup>4-8</sup> The physics of the self-assembling behavior and the microphase-separated nanostructures of diblock copolymers in bulk have been well understood, where the equilibrium nanostructures including lamellae (LAM), hexagonally packed cylinders (HEX), bicontinuous gyroids, and body centered cubic arrays of spheres (BCC) are determined by the volume fraction  $f$  of the individual block and the  $\chi N$  value (where  $\chi$  is the Flory-Huggins interaction parameter and  $N$  is the total polymerization degree of the BCP).<sup>2, 6, 9</sup> However,

the self-assembling behavior and the final structures in thin films of BCPs have some differences from those in bulk as a consequence of both geometric frustration and surface interactions.<sup>4, 10-12</sup>

For BCPs with the lamellar and cylindrical bulk morphologies, how to control the long-range order and the orientation of the nanostructures in thin films has attracted much attention.<sup>4, 12, 13</sup> In order to generate laterally long-range ordered thin films with vertically orientated lamellae and cylinders, many methods have been attempted,<sup>12, 14</sup> including surface neutralization,<sup>15</sup> solvent annealing,<sup>16</sup> directional solidification, and so on.<sup>11, 17, 18</sup> Compared with the lamellar and cylindrical nanostructures, the spheres of the BCC structure do not have anisotropy, and thus the orientation of the BCC structure in thin films is in general less complicated than that of the HEX or LAM structures. For block copolymers with bulk BCC structures, many theoretical and experimental studies have been focused on the order-order and order-disorder transitions induced by the substrate and confinement in thin films.<sup>14, 19-24</sup> Moreover, ordering of the spheres along the direction normal to the substrate in thin films of asymmetric diblock copolymers with relatively larger layer thicknesses was reported,<sup>25</sup> while the spheres were almost short-range ordered in the plane parallel to the substrate.<sup>26</sup> However, the lateral order and ordering range of the BCC

<sup>a</sup> College of Polymer Science and Engineering, State Key Laboratory of Polymer Materials Engineering, Sichuan University, Chengdu 610065, China. E-mail: shilingying@scu.edu.cn.

<sup>b</sup> Beijing National Laboratory for Molecular Sciences, Key Laboratory of Polymer Chemistry and Physics of Ministry of Education, Center for Soft Matter Science and Engineering, College of Chemistry and Molecular Engineering, Peking University, Beijing 100871, China.

† Electronic Supplementary Information (ESI) available: TEM micrographs with high magnifications of the thin films of  $D_{58}B_{104}$  and  $D_{58}B_{82}$  with well-matched [110]-oriented BCC domains; TEM micrograph of the thin film of  $D_{58}B_{40}$  with several domains having defects. See DOI: 10.1039/x0xx00000x

spheres as well as the morphologies at the boundaries of the adjacent ordered domains in thin films of asymmetrical BCP with a thickness within a certain range are rarely investigated.

The diblock copolymer, poly(dimethylsiloxane)-*b*-poly{2,5-bis[(4-butoxyphenyl)oxycarbonyl]styrene} (PDMS-*b*-PBPCS, DB) shown in Fig. 1a is an unusual liquid crystalline (LC) BCP in which the PBPCS is a mesogen-jacketed liquid crystalline polymer (MJLCP) exhibiting an unusual LC phase behavior.<sup>27–29</sup> The DB samples synthesized through atom transfer radical polymerization (ATRP) have well-defined chemical structures and narrow molecular weight distributions indicated by the low polydispersity index (PDI) of less than 1.09.<sup>29</sup> The self-assembling behavior of DB block copolymers with various volume fractions of PDMS ( $f_{\text{PDMS}}$ 's) ranging from 10% to 23% in bulk has been reported in our previous work,<sup>29</sup> and the stable BCC structure and the clearly thermoreversible BCC-HEX transition (as shown in Fig. 1b) have been observed by variable-temperature small-angle X-ray scattering (SAXS) experiments. Surprisingly, for this series of block copolymers with a relatively wide range of  $f_{\text{PDMS}}$  values, the BCC structure is their thermodynamic stable structure in bulk at ambient temperature after the samples are annealed in a temperature range of 130 to 190 °C in which the BCC structure is formed, or after they are annealed at even higher temperatures at which some BCPs transform to the HEX structure.<sup>29</sup>

In this work, we present the micrometer-scale ordered domains of [110]-oriented BCC spheres parallel to the substrate and interesting morphologies at the boundaries of the adjacent [110]-oriented domains in the thin film of the narrowly dispersed DB BCPs with BCC structures in bulk. The thin films of these BCPs with relatively large thicknesses were prepared by solution-casting using carbon-film coated substrates. After the thin films were annealed at appropriate condition, the morphologies were characterized by transmission electron microscopy (TEM) and X-ray photoelectron spectroscopy (XPS).

## Experimental Section

### Materials.

The DB block copolymers were synthesized through the atom transfer radical polymerization (ATRP) method as reported in our previous work.<sup>29</sup> Tetrahydrofuran (THF, Beijing Chemical Reagents Co., A.R.) was used after distillation. The carbon membranes coated on Cu grids (T10044, Beijing XinXing Braim Technology Co., Ltd.) were used as received.

In a typical synthesis of DB block copolymer, the monomer {2,5-bis[(4-butoxyphenyl)oxycarbonyl]styrene} (BPCS) (0.835 g, 1.38 mmol), PDMS-Br (0.06 g, 13.8 μmol), CuBr (1.99 mg, 13.8 μmol), PMDETA (2.40 mg, 13.8 μmol), and chlorobenzene (3.66 mL) were charged into a polymerization tube. The tube was sealed under vacuum after being stirred and degassed by three freeze-pump-thaw cycles, and subsequently immersed into an oil bath maintained at 110 °C for 8 h. It was then quenched in liquid nitrogen and taken out to ambient condition. The solution was passed through a neutral alumina

column in order to remove the copper salt. Finally, the as-synthesized copolymer was precipitated in a large volume of methanol and dried in vacuum overnight.

### Thin-Film Preparation and Characterization.

The DB BCPs were dissolved in dry THF (with concentrations of 2.5–3 mg/mL) with stirring at ambient temperature for 12 h. Then the homogeneous solutions were cast onto carbon membranes coated Cu grids (T10044) in dry air. The thin films were maintained at ambient temperature for 3 days for the solvent to evaporate completely, followed by annealing in vacuum at 180 °C for 3 days h. The film thicknesses of the result thin films were ca. 80–100 nm. Then the morphologies of the thin films were characterized by TEM and XPS. The TEM bright-field images were obtained with a Tecnai G2 F20 instrument using an accelerating voltage of 120 kV. The XPS experiments were carried out on an XSAM800 (Kratos Company, UK) with Al K $\alpha$  radiation ( $h\nu = 1486.6$  eV).

## Results and Discussion

### The Compositions of the Asymmetrical DB BCPs and Their BCC Structures in Bulk after Annealing at 180 °C.

The DB block copolymers used in this work ( $D_{58}B_{104}$ ,  $D_{58}B_{82}$  and  $D_{58}B_{40}$ ) were synthesized through ATRP as reported in our previous work,<sup>29</sup> and their number-averaged molecular weight ( $M_n$ ), polymerization degree, PDI,  $f_{\text{PDMS}}$  values, and glass transition temperatures of PBPCS blocks ( $T_g(\text{PBPCS})$ ) are listed in Table 1. These BCPs have well-defined chemical structures and narrow molecular weight distributions with PDI values less than 1.10.<sup>29</sup> When the DB BCPs are annealed at relatively low temperatures, all of them self-assemble into thermodynamically stable BCC nanostructures in bulk.<sup>29</sup> This work is focused on the microphase-separated morphologies in thin films of these BCPs after annealing at 180 °C at which the BCC structures are stable for these BCPs. The  $d$ -spacing values of the BCC nanostructures of  $D_{58}B_{104}$ ,  $D_{58}B_{82}$  and  $D_{58}B_{40}$  in bulk at ambient temperature after annealing at 180 °C are 20.8, 18.9, and 14.5 nm, respectively.<sup>29</sup> In addition, the  $d$ -spacing values of these BCC nanostructures obtained from the SAXS experiments are  $d_{110}$  values which are equivalent to the  $a/\sqrt{2}$  (where  $a$  is  $d_{100}$ ) values. Thus, the  $a$  values of  $D_{58}B_{104}$ ,  $D_{58}B_{82}$ , and  $D_{58}B_{40}$  are 29.4, 26.7 and 20.5 nm, respectively. For the BCC structure shown by the model in Fig. 2a, the morphologies that can be observed in TEM experiments along the [100], [110] and [111] directions are shown in Fig. 2b–d, respectively. The red and dark red spheres are the real spheres in a single lattice plane, and the grey spheres are the orthographic projection of the spheres in the corresponding neighboring plane. For the [100] zone, the morphology should be square pattern with the nearest sphere-to-sphere distance equivalent to  $a/\sqrt{2}$ . For the [110] zone, the rectangular pattern should have the length equivalent to  $a/\sqrt{2}$  and the width equivalent to  $a/2$ . The [111] zone should have the triangular pattern with the nearest sphere-to-sphere distance equal to  $(\sqrt{2}/\sqrt{3})a$ . Therefore, we can distinguish the orientation of the BCC structure in the thin

films from the morphologies of TEM experiments in the following section.

### Micrometer-Scale Ordered Domain of [110]-Oriented BCC Spheres in Thin Films of $D_{58}B_{104}$ , $D_{58}B_{82}$ , and $D_{58}B_{40}$ BCPs.

The thicknesses of the BCP thin films can be controlled by the concentration and the volume of the solution used for casting a piece of thin film as described in our previous work.<sup>30</sup> In order to avoid the influence of the thin-film thickness on the morphology, we controlled the average thickness of the thin films of the BCPs to be 80–100 nm which were about 5–6 multiples of the periodicities of [110] plane of the BCC structure. The electron density of PDMS ( $\rho_{\text{PDMS}}^e$ ) is larger than that of PBPCS ( $\rho_{\text{PBPCS}}^e$ ), because PDMS contains Si element in addition to C, H, and O elements.<sup>31</sup> Thus, the microphase-separated morphologies of the thin films can be directly distinguished in the TEM micrographs. Moreover, the compositions of the surface layers of the thin films can be determined by XPS experiments.

First, we studied the microphase-separated nanostructures of the thin films of  $D_{58}B_{104}$  after annealing at 180 °C for 3 days. As shown in Fig. 3a, the micrometer-scale domain with a uniform morphology is observed in the TEM experiment. In the TEM micrographs with higher magnifications (Fig. 3b–c), the rectangular arrangement of the dark dots is clearly observed. Because of the higher electron density of PDMS that contains Si element, the darker part in the TEM micrograph is the PDMS domain.<sup>31</sup> In addition, the length and the width of the lattice of the rectangular are equivalent to 20.6 and 14.8 nm, respectively, which are quite consistent with the calculated values ( $a/\sqrt{2} = 20.8$  nm, and  $a/2 = 14.7$  nm) from the model of the [110] zone of the BCC nanostructure as shown in Fig. 3d. The radius of the PDMS sphere of the BCP is calculated to be 6.7 nm from the  $f_{\text{PDMS}}$  value and  $a$  value of the BCC unit cell ( $f_{\text{PDMS}} = 8\pi r^3/3a^3$ , thus  $r = a(3f_{\text{PDMS}}/8\pi)^{1/3}$ ). The width of the rectangular lattice ( $a/2$ ) is 14.7 nm which is larger than the  $2r$  value (13.4 nm), and thus the PDMS dots are separated from each other in the TEM micrograph. Therefore, the morphology of the thin film of  $D_{58}B_{104}$  as shown in Fig. 3 is projection of the BCC structure along the [110] direction.

For the thin film of  $D_{58}B_{82}$ , the micrometer-scale ordered domain with the oriented nanostructure is also observed, as show in Fig. 3e. The TEM micrographs with higher magnifications in Fig. 3f–g clearly display rectangular arrangement of the spheres, which indicate the [110]-orientated BCC spheres of  $D_{58}B_{82}$  on the substrate. In addition, the length and the width of the rectangular lattice are equivalent to 18.6 and 13.6 nm, respectively, which are consistent with the calculated values ( $a/\sqrt{2} = 18.9$  nm and  $a/2 = 13.5$  nm) from the model of the [110] projection as shown in Fig. 3h. The  $2r$  value of the PDMS sphere of  $D_{58}B_{82}$  is calculated to be 13.2 nm, which is a little smaller than the value of the width of the rectangular lattice ( $a/2 = 13.5$  nm), and thus the PDMS dots are still separated from each other in the width direction of the rectangular lattice but are much closer than those of  $D_{58}B_{104}$  in the thin film as shown in the TEM

micrographs. Therefore, the morphology of the thin film of  $D_{58}B_{82}$  shown in Fig. 3 is also the [110] projection of the BCC spheres.

Then, the morphologies of thin film of the  $D_{58}B_{40}$  BCP after annealing at 180 °C for 3 days were characterized. As shown in Fig. 3i–j, the uniformly oriented micrometer-scale domain is observed. The dark PDMS phase even occupies more area than the light PBPCS phase in the TEM image. From the TEM micrograph with a higher magnification (Fig. 3k), it is clearly observed that the dark phase are composed of overlapped PDMS spheres. Thus, the morphology of the thin film of  $D_{58}B_{40}$  is also the BCC structure of the [110]-oriented close packed spheres. In addition, the distance between the neighboring dark phases is measured to be 14.6 nm, which is consistent with the calculated length of the rectangular lattice ( $a/\sqrt{2} = 14.5$  nm) from the model of the [110] projection as shown in Fig. 3l. The radius of the PDMS sphere of the  $D_{58}B_{40}$  BCP is calculated to be 6.2 nm from the  $f_{\text{PDMS}}$  value and the BCC unit cell. Thus, the  $a/2$  value (10.3 nm) is much smaller than the  $2r$  value (12.4 nm) due to the relatively higher  $f_{\text{PDMS}}$  value (23%) of  $D_{58}B_{40}$  BCP. Therefore, the PDMS spheres observed along the [110] direction are overlapped with each other, consistent with the TEM result.

The solubility parameters of PBPCS and PDMS are 21.8 and 15.0  $\text{J}^{1/2}\text{cm}^{-3/2}$ , respectively,<sup>29,32</sup> indicating that DB is a kind of strong microphase-separated BCP and the surface energy of PDMS is lower than that of PBPCS. The substrate surface, low-surface-energy carbon thin film,<sup>33</sup> has no distinct preferential interaction with PDMS or PBPCS, and thus is a relatively neutral surface for these BCPs. In order to determine the composition of the surface layer of these thin films, XPS experiments were carried out. The XPS profiles of  $D_{58}B_{104}$ ,  $D_{58}B_{82}$ , and  $D_{58}B_{40}$  are shown in Fig. 4. In each curve, three groups of characteristic signals from carbon, oxygen, and silicon are clearly observed. First, the O 1s peak at a binding energy of 532 eV, and the C1s peak at a binding energy of 284–289 eV are observed, originating from both PDMS and PBPCS. And the Si 2s and Si 2p binding peaks appear at 152 and 102 eV, respectively. Comparing the relative intensities of the Si 2s and Si 2p binding peaks of the three BCPs with different  $f_{\text{PDMS}}$  values, the content of PDMS increases as  $f_{\text{PDMS}}$  increases. In addition, the mole ratios of PDMS to PBPCS in the surface layers can be calculated from the C:O ratio from the XPS results, and the calculated compositions of the surface layers of the thin films are almost consistent with the composition of the corresponding block copolymers. Therefore, the surface layer is also composed of both PDMS and PBPCS blocks, without significant accumulation of PDMS, which may be ascribed to the low  $f_{\text{PDMS}}$  values and the stability of BCC nanostructures of these BCPs.

All thin films of these DB BCPs with  $f_{\text{PDMS}}$  values of 10%, 13%, and 23% present micrometer-scale domains of [110]-oriented BCC spheres. First of all, PDMS is the minor phase and the BCC structures are the thermodynamically stable nanostructures for these DB BCPs.<sup>29</sup> And these thin films were annealed at an appropriate temperature (180 °C) for a relatively long time (3 days) which enabled the BCPs to self-

assemble into the thermodynamically stable nanostructure.<sup>34</sup> Thus, the microphase-separated nanostructures of these BCPs thin films with relatively large thicknesses are still BCC structures. Secondly, the orientation of the BCC structure with the close-packed [110] planes parallel to substrates can minimize the amount of chain stretching required to fill the interstitial space at the substrate and free interfaces. **Fig. 5a-c** illustrate the chain arrangements of the DB block copolymer in a single [100], [110], and [111] plane of the BCC structure, respectively. In order to fill the interstitial space, the PBPCS chains in the [100] and [111] planes stretch more compared with those in the [110] plane. Moreover such a [110] orientation is consistent with the results reported in literature.<sup>19, 23, 25</sup> Thirdly, PDMS has a relatively low-surface energy,<sup>32</sup> and the [110] orientation can maximize the occupation of the PDMS chains at the substrate and free interfaces (the occupation ratios of PDMS in the [100], [110], and [111] plane are  $\pi r^2/a^2$ ,  $\sqrt{2}\pi r^2/a^2$  and  $\pi r^2/\sqrt{3}a^2$ , respectively, where  $r$  is the radius of the PDMS sphere and the  $a$  is  $d_{100}$ ). Moreover, these DB BCPs are narrowly dispersed with PDI < 1.10, thus relatively long-range ordering of the domains can be achieved. Therefore, all thin films of these DB BCPs have the BCC nanostructures with the preferential [110]-orientation parallel to the substrate, and extraordinarily, the size of the [110]-oriented domain in this work is on the micrometer scale. Moreover, multiple [110]-oriented domains can join together to form even larger ordered domains. And the morphology at the boundaries of two or more adjacent [110]-oriented BCC domains will be of great interest.

#### Interesting Morphologies at the Boundaries of Adjacent [110]-Oriented BCC Domains in Thin Films of $D_{58}B_{104}$ , $D_{58}B_{82}$ , and $D_{58}B_{40}$ BCPs.

After the morphologies of the single, large-scale [110]-oriented BCC domains of the thin films of these BCPs were studied, the morphologies at the boundaries of adjacent [110]-oriented BCC domains were investigated. For the thin films of  $D_{58}B_{104}$  and  $D_{58}B_{82}$  BCPs, the adjacent [110]-oriented domains match each other quite well, as shown in **Fig. 6** illustrating several domains of the [110]-oriented BCC structures in the TEM micrographs of thin films of  $D_{58}B_{104}$  and  $D_{58}B_{82}$ . The boundaries of the adjacent [110]-oriented domains of these two BCPs are indicated with dashed lines, and clearly there are no obvious defects observed at the boundaries in the TEM micrograph. In addition, magnified TEM images of the  $D_{58}B_{104}$  and  $D_{58}B_{82}$  thin films with two well matched [110]-oriented domains are shown in **Fig. S1**, and the arrangement of the PDMS dots of the neighboring domains near the interface is illustrated by the model shown in the inset of each micrograph. The neighboring [110] domains share a twin plane and do not influence the ordering and arrangement of the spheres of each other. The morphology of each boundary observed in the TEM micrographs is almost a line with no defects. Thus, the boundaries of the adjacent [110]-oriented domains in thin films of the  $D_{58}B_{104}$  and  $D_{58}B_{82}$  BCPs are almost 'defect-free interfaces'.

For the thin films of  $D_{58}B_{40}$ , the morphologies at the boundaries of the adjacent [110]-oriented domains are more complicated but interesting. As shown in **Fig. 7a**, the boundaries of the two neighboring [110] domains is also defect-free interface which is similar to the case of the  $D_{58}B_{104}$  and  $D_{58}B_{82}$  BCPs. The two neighboring [110]-oriented BCC domains are symmetrically oriented, and the morphological pattern of the TEM micrograph in **Fig. 7a** is illustrated by the model shown in **Fig. 7b** in which  $\theta_1 \approx \theta_2$ . A second case is the asymmetrical arrangement of two neighboring [110]-oriented BCC domains as shown in **Fig. 7c**, the twin BCC spherical domains do not match each other at the twin plane, and the line defects at the interface marked by the dashed lines are observed. Because PDMS contains the Si element with a higher electron density compared with C and H atoms,<sup>29, 31</sup> the darker dots both in the [110]-orientated domains and at the interface in the TEM micrograph are the PDMS microdomains. The arrangement of the PDMS dots in the TEM micrograph (**Fig. 7c**) is illustrated by the model shown in **Fig. 7d**. Because  $\theta_3 \approx 2\theta_4$  which leads to  $OB \approx 2OA$ , the PDMS dots are redundant at those B and O sites of the interface as indicated by the circles in the model. Thus, the enrichment of PDMS at the interface leads to the rearrangement of the PDMS phase at the interface which results in the line defects.

Moreover, there are some new morphologies with more interesting boundaries observed in thin films of  $D_{58}B_{40}$ . As shown in **Fig. 8a**, the twin BCC-sphere A and B domains with matching lattices at the twin plane along with the domain C which is a boundary of several [110]-oriented BCC domains are observed. In addition, many domains with the same morphological characteristics as those of domain C are observed in the thin film of  $D_{58}B_{40}$  as shown in **Fig. S2†** in ESI. In order to investigate the morphological characteristics of domain C, the TEM experiments for structural determination at tilting angles of 0–30° were performed,<sup>35</sup> and the results are shown in **Fig. 8b–f**. The red circle indicating the joint of the domains A, B and C was used as the marker in the TEM tilting experiments. With the increase in the tilting angle, there are some changes in the morphology. When the tilting angle is increased to 25° and 30°, the area in the white box shows the characteristics of the [110]-oriented BCC morphology, but the other areas in domain C are still disordered. Therefore, the domain C is dominated with defects but has local ordering of the BCC structure. By the way, the orientation of the BCC structure and the pattern of the PDMS dots on the TEM micrographs in the [110]-orientated domain A and B are illustrated by the model in **Fig. S3a–b**. After tilting 30°, the morphologies of domain A and B are consistent with theoretical patterns for the corresponding [110]-oriented domain with ordered BCC structures after the same tilting (**Fig. S3a'–b'**), which further indicates the ordering of the BCC structure in the [110]-oriented domains.

Thus, the morphologies at the boundaries of the neighboring [110]-oriented BCC domains in thin films of  $D_{58}B_{40}$  BCP include interfaces without defects, interfaces with line defects, and domains with defects and local ordering. The formation of these different morphological boundaries with

more defects in thin films of  $D_{58}B_{40}$  can be attributed to the relatively high volume fraction occupied by PDMS spheres. For  $D_{58}B_{40}$  with a higher  $f_{PDMS}$  value of 23%, the homogeneous nucleation of the PDMS blocks to form the BCC structure will be much easier than that of  $D_{58}B_{104}$  and  $D_{58}B_{82}$ . When two [110]-orientated domains in thin films of  $D_{58}B_{40}$  are developed and encounter with each other, the mismatching, overlapping, and rearrangement of the PDMS spheres are much easier to occur at the interfaces. Thus, only when the two neighboring domains symmetrically re-arrange, will the boundary be the defect-free interface; otherwise the boundary of the interface with defects will appear. Once the mismatching or overlapping develops at the end of the interface of the two neighboring [110]-orientated domains, a new domain with defects and local ordering of the BCC structure will generate until stopped by other [110]-orientated domains already developed. But for the  $D_{58}B_{104}$  and  $D_{58}B_{82}$  with relatively lower  $f_{PDMS}$  values, the encountered [110] domains can be much easier to accommodate to each other, and the boundaries are simply interfaces. Therefore, there are more defects at the boundaries in thin films of  $D_{58}B_{40}$  than those in thin films of  $D_{58}B_{104}$  and  $D_{58}B_{82}$ .

Moreover, the above study on the boundary morphologies of the adjacent [110]-oriented BCC domains of DB thin films indicates that once a BCC structure forms, the micrometer-scale [110]-oriented BCC domain develops under thermal annealing control. In order to attain more long-ranged structure, "zone-annealing"<sup>36</sup> method might be effectively used to remove the interfaces and the thin film with a single large [110]-oriented BCC domain especially for  $D_{58}B_{104}$  and  $D_{58}B_{82}$  might be developed in our future work.

## Conclusions

In summary, the microphase separation and structure orientation in thin films of a series of asymmetrical DB BCPs with thermodynamically stable bulk BCC structures are investigated utilizing TEM and XPS. The thin films with relatively large thickness were prepared on carbon film-coated substrates and were annealed in vacuum at 180 °C for 3 days. All thin films of these DB BCPs with  $f_{PDMS}$  values ranging from 10% to 23% have a common characteristic that the BCC structures prefer to orient with the [110] plane parallel to the substrate because this orientation can minimize the extent of chain stretching required to fill the interstitial space at the substrate and free interfaces, and can maximize the occupation of PDMS at the substrate and free interfaces. The uniform domain with the [110]-oriented BCC structure in all thin films is on the micrometer scale. For the thin films of the BCPs with relatively low  $f_{PDMS}$  values ( $D_{58}B_{104}$  and  $D_{58}B_{82}$ ), the adjacent [110]-oriented BCC domains match each other well, and the boundaries are almost defect-free interfaces. For the thin film of  $D_{58}B_{40}$  which has a relatively high  $f_{PDMS}$  value, various morphologies at the boundaries are observed including defect-free interfaces, interfaces with line defects, and domains with defects and local ordering. The long-range ordering of the [110]-oriented BCC structure and the well

matching of the neighboring [110] domains can be ascribed to the well-defined chemical structure and narrow polydispersity of these BCPs. The increase in the number of the defects at the boundaries of adjacent [110] domains in the thin film of  $D_{58}B_{40}$  is attributed to the accumulation of PDMS spheres at the interfaces because of the increase in the volume fraction occupied by the PDMS spheres. Moreover, the  $D_{58}B_{104}$  and  $D_{58}B_{82}$  BCPs have thermoreversible BCC-HEX order-order transitions at higher temperatures in bulk, and the further researches on the phase transition behaviors of the thin films as well as the "zone-annealing" method used to generate better long-range ordered thin films of these BCPs will be conducted in our future work. Furthermore, the thin films of these BCPs with long-range ordering are possible candidates for nano-templates.

## Acknowledgements

Financial support from the National Natural Science Foundation of China (Grant 51403132 and 20874003) is gratefully acknowledged.

## Notes and references

- (a) M. Muthukumar, C. K. Ober and E. L. Thomas, *Science* 1997, **277**, 1225; (b) A.-V. Ruzette and L. Leibler, *Nat. Mater.* 2005, **4**, 19; (c) R. Deng, F. Liang, P. Zhou, C. Zhang, X. Qu, Q. Wang, J. Li, J. Zhu and Z. Yang, *Adv. Mater.* 2014, **26**, 4469.
- T. P. Lodge, *Macromol. Chem. Phys.* 2003, **204**, 265.
- (a) Y. Mai and A. Eisenberg, *Chem. Soc. Rev.* 2012, **41**, 5969; (b) H. Xu, D. Chen, S. Wang, Y. Zhou, J. Sun, W. Zhang and X. Zhang, *Philosophical Transactions of the Royal Society of London A: Mathematical, Physical and Engineering Sciences*, 2013, **371**, 20120305.
- I. W. Hamley, *Prog. Polym. Sci.* 2009, **34**, 1161.
- (a) Y. Lei, S. Yang, M. Wu and G. Wilde, *Chem. Soc. Rev.* 2011, **40**, 1247; (b) Q. Liu, Z. Tang, B. Ou, L. Liu, Z. Zhou, S. Shen and Y. Duan, *Mater. Chem. Phys.* 2014, **144**, 213.
- F. S. Bates and G. H. Fredrickson, *Phys. Today* 1999, **52**, 32.
- (a) A. del Campo and E. Arzt, *Chem. Rev.* 2008, **108**, 911; (b) J. Shen, C. Chen, W. Fu, L. Shi and Z. Li, *Langmuir*, 2013, **29**, 6271; (c) S.-J. Jeong, H.-S. Moon, J. Shin, B. H. Kim, D. O. Shin, J. Y. Kim, Y.-H. Lee, J. U. Kim and S. O. Kim, *Nano Lett.* 2010, **10**, 3500; (d) N. Ma, Y. Li, H. Xu, Z. Wang and X. Zhang, *J. Am. Chem. Soc.* 2009, **132**, 442; (e) J. Zhang and C. M. Li, *Chem. Soc. Rev.* 2012, **41**, 7016; (f) Q. Zhang, Z. Fang, Y. Cao, H. Du, H. Wu, R. Beuerman, M. B. Chan-Park, H. Duan and R. Xu, *ACS Macro Lett.* 2012, **1**, 876.
- For comparison with the coordination-polymer templates for nano- and microfabrication, one may refer to: X. Liu, *Angew. Chem. Int. Ed.* 2009, **48**, 3018.
- M. W. Matsen and F. S. Bates, *Macromolecules* 1996, **29**, 1091.
- J. N. L. Albert and T. H. Epps III, *Mater. Today* 2010, **13**, 24.
- S. H. Kim, M. J. Misner and T. P. Russell, *Adv. Mater.* 2008, **20**, 4851.
- J. Bang, U. Jeong, D. Y. Ryu, T. P. Russell and C. J. Hawker, *Adv. Mater.* 2009, **21**, 4769.
- J. Y. Cheng, A. M. Mayes and C. A. Ross, *Nat. Mater.* 2004, **3**, 823.
- M. J. Fasolka and A. M. Mayes, *Annu. Rev. Mater. Res.* 2001, **31**, 323.

- 15 K. W. Guarini, C. T. Black and S. H. I. Yeung, *Adv. Mater.* 2002, **14**, 1290.
- 16 J. Bang, S. H. Kim, E. Drockenmuller, M. J. Misner, T. P. Russell and C. J. Hawker, *J. Am. Chem. Soc.* 2006, **128**, 7622.
- 17 R. A. Segalman, *Science* 2008, **321**, 919.
- 18 S. Park, D. H. Lee, J. Xu, B. Kim, S. W. Hong, U. Jeong, T. Xu and T. P. Russell, *Science* 2009, **323**, 1030.
- 19 G. E. Stein, E. J. Kramer, X. Li and J. Wang, *Macromolecules* 2007, **40**, 2453.
- 20 Y. Qiao, R. Ferebee, B. Lee, I. Mitra, N. A. Lynd, J. Hayat, G. E. Stein, M. R. Bockstaller and C. Tang, *Macromolecules* 2014, **47**, 6373.
- 21 M. Komura, H. Komiyama, K. Nagai and T. Iyoda, *Macromolecules* 2013, **46**, 9013.
- 22 N. Sota, K. Saijo, H. Hasegawa, T. Hashimoto, Y. Amemiya and K. Ito, *Macromolecules* 2013, **46**, 2298.
- 23 G. E. Stein, E. W. Cochran, K. Katsov, G. H. Fredrickson, E. J. Kramer, X. Li and J. Wang, *Phys. Rev. Lett.* 2007, **98**, 158302.
- 24 H. Tan, M. Zhang, Y. Deng, Q. Song and D. Yan, *Polymer* 2013, **54**, 6853.
- 25 H. Yokoyama, E. J. Kramer, M. H. Rafailovich, J. Sokolov and S. A. Schwarz, *Macromolecules* 1998, **31**, 8826.
- 26 H. Yokoyama, T. E. Mates and E. J. Kramer, *Macromolecules* 2000, **33**, 1888.
- 27 Y.-F. Zhao, X.-H. Fan, X.-H. Wan, X.-F. Chen, Yi, L.-S. Wang, X. Dong and Q.-F. Zhou, *Macromolecules* 2006, **39**, 948.
- 28 X.-F. Chen, Z. Shen, X.-H. Wan, X.-H. Fan, E.-Q. Chen, Y. Ma and Q.-F. Zhou, *Chem. Soc. Rev.* 2010, **39**, 3072.
- 29 L.-Y. Shi, I. F. Hsieh, Y. Zhou, X. Yu, H.-J. Tian, Y. Pan, X.-H. Fan and Z. Shen, *Macromolecules* 2012, **45**, 9719.
- 30 L.-Y. Shi, Y. Zhou, Z. Shen and X.-H. Fan, *Macromolecules* 2012, **45**, 5530.
- 31 G. H. Michler, in *Electron Microscopy of Polymers*, Springer-Verlag, Berlin, 2008.
- 32 A. F. M. Barton, in *Handbook of Solubility Parameters and Other Cohesion Parameters*, 2nd ed., CRC Press, Florida, 1983.
- 33 L. Tsarkova, A. Knoll, G. Krausch and R. Magerle, *Macromolecules* 2006, **39**, 3608.
- 34 (a) M. P. Stoykovich, H. Kang, K. C. Daoulas, G. Liu, C.-C. Liu, J. J. de Pablo, M. Müller and P. F. Nealey, *ACS Nano* 2007, **1**, 168; (b) P. F. Green and R. Limary, *Adv. Colloid Interface Sci.* 2001, **94**, 53.
- 35 (a) I. F. Hsieh, H.-J. Sun, Q. Fu, B. Lotz, K. A. Cavicchi and S. Z. D. Cheng, *Soft Matter* 2012, **8**, 7937; (b) C. De Rosa, C. Park, B. Lotz, J.-C. Wittmann, L. J. Fetters and E. L. Thomas, *Macromolecules* 2000, **33**, 4871.
- 36 (a) B. C. Berry, A. W. Bosse, J. F. Douglas, R. L. Jones and A. Karim, *Nano Lett.* 2007, **7**, 2789; (b) P. W. Majewski and K. G. Yager, *ACS Nano* 2015, **9**, 3896.